RESEARCH ARTICLE | JANUARY 26 2026

Spectral statistics of preferred orientation quantum graphs

Ram Band ; Pavel Exner ; Divya Goel ; Aviya Strauss

J. Math. Phys. 67, 013502 (2026)
https://doi.org/10.1063/5.0295424

Journal of Mathematical Physics ARTICLE pubs.aip.org/aip/jmp

Spectral statistics of preferred orientation quantum graphs

Cite as: J. Math. Phys. 67, 013502 (2026); doi: 10.1063/5.0295424
Submitted: 8 August 2025 • Accepted: 31 December 2025 •
Published Online: 26 January 2026

Ram Band,[1,a] Pavel Exner,[2,3] Divya Goel,[4] and Aviya Strauss[5]

AFFILIATIONS

[1] Department of Mathematics, Technion–Israel Institute of Technology, Haifa, Israel
[2] Doppler Institute, Czech Technical University, Prague, Czechia
[3] Nuclear Physics Institute, Czech Academy of Sciences, Řež, Czechia
[4] Department of Mathematical Sciences, Indian Institute of Technology (BHU), Varanasi 221005, India
[5] Faculty of Electrical and Computer Engineering, Technion–Israel Institute of Technology, Haifa, Israel

[a] Author to whom correspondence should be addressed: ramband@technion.ac.il

ABSTRACT

We study the spectral statistics of quantum (metric) graphs whose vertices are equipped with preferred orientation vertex conditions. When comparing their spectral statistics to those predicted by suitable random matrix theory ensembles, one encounters some deviations. We point out these discrepancies and demonstrate that they occur in various graphs and even for Neumann-Kirchhoff vertex conditions, which was overlooked so far. Detailed explanations and computations are provided for this phenomenon. To achieve this, we explore the combinatorics of periodic orbits, with a particular emphasis on counting Eulerian cycles.

I. INTRODUCTION

Since the seminal paper of Kottos and Smilansky[48] it is known that quantum graphs[9,11,19,36,47,52] are a suitable class of systems on which chaotic properties can be tested. One of the accepted conclusions is that the spectral statistics of quantum graphs fall into several universal classes, in particular, that the *Gaussian Orthogonal Ensemble* (GOE) distribution can be observed only if the system exhibits invariance with respect to the time reversal. One aim of this paper is to challenge this "rule" by providing examples of graphs having the GOE eigenvalue statistics despite being time-reversal asymmetric.

To give an example, one may consider a quantum particle living on an *octahedron* of incommensurate edge lengths assuming that the boundary values of the wavefunctions and their derivatives at each vertex are matched through the conditions,

$$\psi_{j+1} - \psi_j + i(\psi'_{j+1} + \psi'_j) = 0, \quad j = 1,2,3,4 \ (\mathrm{mod}\ 4), \tag{1.1}$$

which are obviously non-invariant with respect to complex conjugation that represents time reversal.

We denote by $\{k_n\}_{n=1}^{\infty}$ the square roots of the eigenvalues of such a quantum graph (see a detailed description of the model in Sec. II). First, we consider the nearest-neighbour spacing distribution which is given by

$$P(x) = \lim_{N\to\infty} \frac{1}{N} \sum_{i=1}^{N} \delta(x - (k_{i+1} - k_i)). \tag{1.2}$$

The nearest-neighbour distribution of an octahedron graph with incommensurate edge lengths follows the Gaussian Orthogonal Ensemble (GOE), as is shown in Fig. 1.

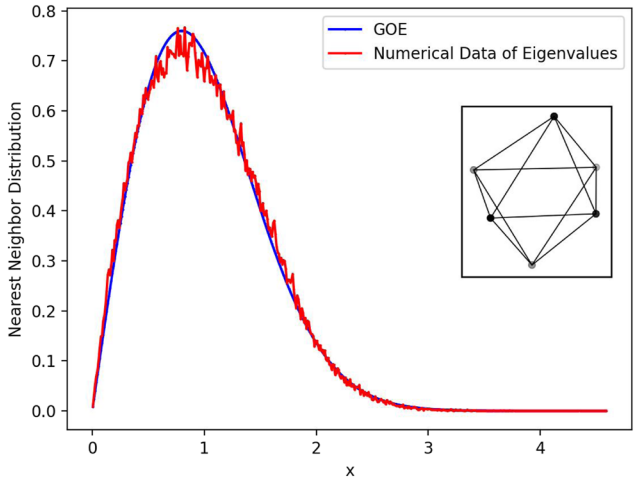

FIG. 1. The nearest-neighbour distribution of the first 4×10^5 eigenvalues of an octahedron graph with incommensurate edge lengths and preferred orientation vertex conditions, (1.1).

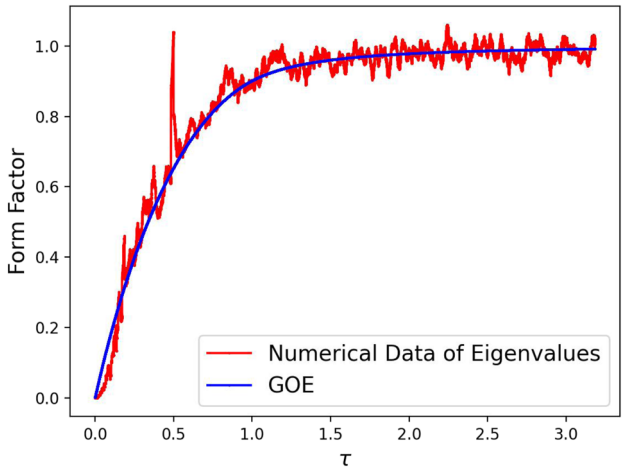

FIG. 2. The form factor of the octahedron graph with incommensurate edge lengths and preferred orientation vertex conditions, (1.1). The numerics was done using eigenvalues no. 5×10^4–1.5×10^5.

The condition (1.1) and its extensions have further interesting consequences for the nearest-neighbour distributions, as we will show in Sec. III and explain in Sec. IV.

Furthermore, when going beyond nearest-neighbour distribution, one considers the two-point correlation function,

$$R_2(x) = \lim_{N\to\infty} \frac{1}{N} \sum_{i=1}^{N} \sum_{j=1}^{N} \delta(x - (k_j - k_i)). \tag{1.3}$$

The Fourier transform of $R_2(x)$ is called the form factor,

$$K(\tau) = \int_{-\infty}^{\infty} e^{2\pi i x \tau} (R_2(x) - 1)\, dx. \tag{1.4}$$

From a global viewpoint, the form factor of the same octahedron graph also exhibits GOE like behaviour. Nevertheless, there is a clear deviation from GOE in the form of a sharp peak at $\tau = 1/2$, as is shown in Fig. 2.

To the best of our knowledge, this specific deviation from the form factor was never mentioned before in the literature. We explain this phenomenon in Sec. V, by providing the required analysis of the form factor. Additionally, we discuss the extensions of these phenomena to other graphs and other vertex conditions.

In Sec. II, we describe in more detail the model and the background in random matrix theory.

II. THE MODEL AND SOME BACKGROUND

A. Graphs with preferred orientation conditions

The motion on the graph edges is free, being described by the Laplacian, $\psi_j \mapsto -\psi_j''$; the nontrivial part comes from the conditions matching the wave functions at the vertices. We write the boundary values at each vertex v as columns, $\Psi(v) := \{\psi_j(v)\}$ and $\Psi'(v) := \{\psi_j'(v)\}$, understood as limits at the endpoint; then the most general way to make the Laplacian a self-adjoint operator is to require

$$(U - I)\Psi(v) + \mathrm{i}(U + I)\Psi'(v) = 0, \tag{2.1}$$

where U is an auxiliary unitary $d \times d$ matrix (d being the degree of the vertex). The origin of this formulation of the vertex conditions is usually referred to Ref. 49 but in fact they appeared already in Ref. 60.

We work with a simple preferred-orientation coupling proposed in Ref. 29 in which

$$U = \begin{pmatrix} 0 & 1 & 0 & \dots & \dots & 0 \\ 0 & 0 & 1 & \ddots & & \vdots \\ \vdots & & 0 & \ddots & 0 & \vdots \\ \vdots & & & \ddots & 1 & 0 \\ 0 & \dots & & & 0 & 1 \\ 1 & 0 & \dots & & \dots & 0 \end{pmatrix} \tag{2.2}$$

is a *circulant matrix*.[25] As an example, writing (2.1) for a degree four vertex in components we get the conditions (1.1). The on-shell scattering matrix at a vertex described by the conditions (2.1) is

$$S(k) = \frac{k - 1 + (k + 1)U}{k + 1 + (k - 1)U}; \tag{2.3}$$

[where if one wants to choose a different length scale (i.e., change units), it is enough to replace k by $k\ell$ for a fixed value $\ell > 0$].

It is easy to check that the S-matrix (2.3) is *not invariant with respect to transposal*, which implies in our case that the transport through the vertex *not* being time-reversal invariant.[30]

To complement the description above, we mention the case of Neumann-Kirchhoff vertex conditions, in which the scattering matrix $S(k)$ is independent of k and its entries equal $[S(k)]_{i,j} = 2/d - \delta_{i,j}$ for a vertex of degree d. Later in the paper we compare results obtained with preferred orientation vertex conditions with results obtained for Neumann-Kirchhoff vertex conditions.

B. Spectral statistics of quantum graphs and random matrix theory–existing results

A driving force in connecting the spectral statistics of chaotic systems to random matrix theory (RMT) lies in the Bohigas–Giannoni–Schmit (BGS) conjecture.[12] In the realm of quantum graphs the conjecture says that the spectral statistics of graphs with incommensurate edge lengths and "sufficient connectivity" exhibits universal statistical properties governed by random matrix theory. Moreover, the symmetry class to which the graphs belong dictates which RMT ensemble describes their spectral statistics. This is still somewhat vague phrasing and substantial effort was made in order to even formalize this conjecture and specify the exact conditions for its validity (both for quantum graphs and for other system within quantum chaos). The connection between quantum graph spectral statistics and RMT was first investigated by Kottos and Smilansky,[48,50] and later extended in works with Schanz,[51,61,62] where spectral fluctuations were analyzed using combinatorial methods (see also Ref. 36 for an extensive review of these results and the ones which follow). Barra and Gaspard[10] contributed a careful study of the nearest-neighbour spacing distribution, helping to establish statistical links with RMT. Tanner[64,65] introduced unitary-stochastic matrix ensembles for classifying when graphs display RMT-like behavior. In particular, he conjectured that the RMT-like behavior is observed if the spectral gap of a certain transition matrix closes slow enough. Berkolaiko and Keating explored spectral statistics in star graphs (where the aforementioned condition is violated),[6,18] and Berkolaiko, in part with Schanz and Whitney, refined these methods analyzing form factors via periodic orbit expansions and diagrammatic approaches.[7,8,20,21] Bolte and Harrison studied spectral statistics for the spin-orbit coupling and for the Dirac operator on graphs.[13–15]

Additional analysis have been obtained using field-theoretic and supersymmetric approaches. In particular, Gnutzmann and Altland[32,33] applied the nonlinear sigma model to show that spectral correlations of individual quantum graphs match RMT predictions. These techniques were further developed by Pluhař and Weidenmüller,[56–58,67] who established RMT universality using diagrammatic and supersymmetric formulations.

Further theoretical works have continued refining the boundary between the classical connection to RMT symmetry classes and its breakdown. Joyner, Müller, and Sieber,[46] as well as Akila and Gutkin,[2,3] showed that systems without spin can still yield GSE-type spectral

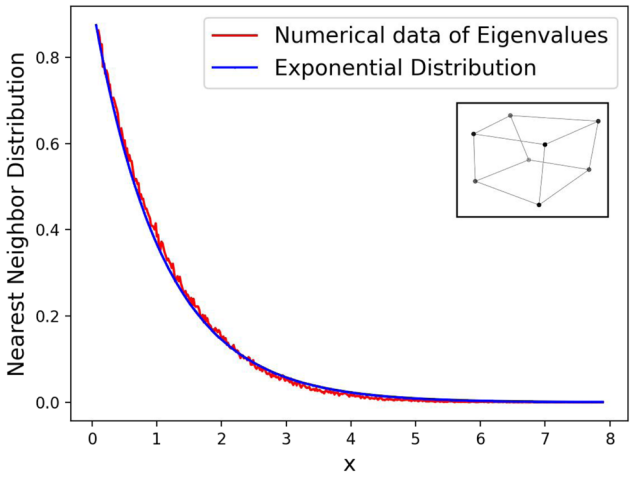

FIG. 3. The nearest-neighbour distribution of the first 2×10^5 eigenvalues of a cube graph with incommensurate edge lengths and preferred orientation vertex conditions.

statistics. Harrison, Swindle, and Winn showed intermediate spectral statistics for various models.[44,45] Band, Harrison, Hudgins, Joyner, and Sepanski studied the variance of coefficients of the characteristic polynomial of the quantum evolution operator[16,17,40,41] (appearing already in the earlier works of Tanner mentioned above). Most recently, Gnutzmann and Smilansky[38] emphasized that RMT-like spectral statistics do not necessarily indicate chaotic classical dynamics.

On the experimental side, realizations of quantum graphs have played a crucial role both in validating RMT connections and in showing deviations from them.[24,26,27,31,39,42,43,53,59]

III. NUMERICAL RESULTS FOR NEAREST NEIGHBOUR DISTRIBUTION

Together with the numerical results shown in the introduction (Fig. 1) for the octahedron graph we also consider other graphs and/or couplings in order to better elucidate the mechanism responsible for the observed effects. First of all, let us note that the eigenvalue counting function of a finite graph with arbitrary self-adjoint vertex conditions satisfies Weyl's law, $N(k) = \frac{L}{\pi}k + \mathcal{O}(1)$ as $k \to \infty$, where $L = \sum_j \ell_j$ is the sum of all the edge lengths. This is known theoretically first from Ref. 50 and later in Ref. 5, prop. 4.2 for the most general self-adjoint conditions (including the preferred orientation conditions which we consider here). As a consequence, the unfolding is trivial; the proper scale to display the eigenvalue spacing is given by the simply scaled momentum variable $\frac{L}{\pi}k$.

We return to Fig. 1 which shows that the nearest neighbour distribution of an octahedron graph is GOE. Modifying the vertex degree can change the spectral picture completely; to illustrate that, we show in Fig. 3 the eigenvalue spacing distribution for a cube graph with incommensurate edge lengths and the same vertex coupling (1.1). In this case we observe that the distribution is of the Poisson type.

Furthermore, it is not so much the vertex degree that determines the statistics type, but rather the presence or absence of the eigenvalue -1 in the spectrum of the matrix U in (2.2). To illustrate this claim, consider the octahedron again, but replace now the coupling (2.2) with a "distorted" one referring to the modified matrix

$$U = \mathrm{e}^{\mathrm{i}\mu}\begin{pmatrix} 0 & 1 & 0 & 0 \\ 0 & 0 & 1 & 0 \\ 0 & 0 & 0 & 1 \\ 1 & 0 & 0 & 0 \end{pmatrix}, \tag{3.1}$$

for some $\mu > 0$. Figure 4 shows that even if the parameter μ is small, the modification changes the picture completely; instead of the GOE we have the Poisson distribution. To be exact, in the numerics the distribution becomes Poissonian if we consider a sufficiently wide energy interval; before we reach this regime one observes a mixture between GOE and Poisson.

IV. DISCUSSION OF THE NEAREST NEIGHBOUR DISTRIBUTION

A. High energy asymptotic of the unitary evolution operator

The occurrence of Poisson distribution in Figs. 3 and 4 is not surprising. In both cases the eigenvalue -1 is missing in the spectrum of the matrix U determining the coupling, and as a result, we get $\lim_{k\to\infty} S(k) = I$ from (2.3). This means that the considered graph turns at high energies effectively into a union of disconnected edges with Neumann endpoints.

The existence of the GOE distribution in Fig. 1 might be less obvious but to understand it one has to realize that while the time-reversal symmetry is violated for any k, the degree of the violation varies. We refer to [Ref. 29, Eq. (5)], in which the entries of the matrix (2.3) were

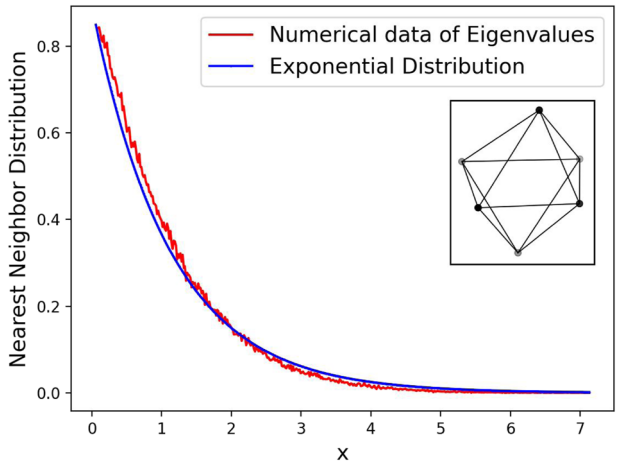

FIG. 4. The nearest-neighbour distribution of the first 2×10^5 eigenvalues of an octahedron graph with incommensurate edge lengths and distorted preferred orientation vertex conditions, (3.1) for $\mu = 0.01$.

expressed as

$$S_{i,j}(k) = \frac{1-\eta^2}{1-\eta^d}\left\{-\eta\frac{1-\eta^{d-2}}{1-\eta^2}\delta_{i,j} + (1-\delta_{i,j})\eta^{(j-i-1) \bmod d}\right\}, \tag{4.1}$$

where $\eta := \frac{1-k}{1+k}$. From here, one can check that the S-matrix of a vertex of even degree d has in the high-energy limit the entries

$$S_{i,j} = -\frac{2}{d}(-1)^{i+j} + \delta_{i,j}, \tag{4.2}$$

which differ from their Neumann-Kircchoff counterparts only by sign on the diagonal and the "even" (i.e., even $i+j$) off-diagonals.

If the vertex is of odd degree then at high energy asymptotics there is an effective decoupling of this vertex into d disjoint vertices of degree one each with Neumann-Kirchhoff conditions, i.e., $S_{i,j} = \delta_{i,j}$.

In both cases (even and odd degrees) the limiting matrix is transpose invariant. Hence, even though the time reversal invariance is violated at any finite energy, it does survive asymptotically. For an even d, in addition, the edges remain coupled asymptotically, which is the reason for the GOE statistics for graphs with even degree vertices and preferred orientation vertex conditions (such as the octahedron considered in Fig. 1. We supplement this observation with a quantitative discussion of the time reversal invariance.

B. On measuring the time reversal invariance violation

The natural measure of time-reversal invariance violation says how much the S-matrix differs from its transpose. We are able to express the violation measure quantitatively by defining

$$\mathcal{M}(k) := \|S(k) - S(k)^T\|, \tag{4.3}$$

from the unitarity of $S(k)$ and the triangle inequality we conclude that the norm cannot exceed two. We employ (4.1) and write the matrix elements of $M(k) = S(k) - S(k)^T$ at a vertex of degree d as

$$M_{ij}(k) = \frac{1-\eta^2}{1-\eta^d}\left\{\eta^{(j-i-1) \bmod d} - \eta^{(i-j-1) \bmod d}\right\}. \tag{4.4}$$

To indicate the dependence on the vertex degree, we add the index d to the symbol $\mathcal{M}$, in what follows. For convenience we will consider separately the prefactor $P_d = \frac{1-\eta^2}{1-\eta^d}$ and the matrix T, whose entries are given by the curly bracket. Being a difference of circulant matrices, T is also circulant which means that its eigenvalues can be expressed explicitly,

$$\lambda_n(\eta) = \sum_{j=1}^{d-1}\left(\eta^{j-1} - \eta^{d-j-1}\right)\omega^{jn}, \quad n = 0, \ldots, d-1, \tag{4.5}$$

where $\omega := \mathrm{e}^{2\pi i/d}$, and in particular, we have $\lambda_0 = 0$. The norm of T is naturally $\|T\| = \max_{0\le n\le d-1}|\lambda_n(\eta)|$.

Being primarily interested in the high-energy behavior of $\mathcal{M}_d(k)$, we have to distinguish the even and odd values of d. The prefactor equals

$$P_{2m}(\eta) = \frac{1}{1+\eta^2+\cdots+\eta^{2m-2}},\ P_{2m+1}(\eta) = \frac{1+\eta}{1+\eta+\cdots+\eta^{2m}}, \tag{4.6}$$

which, translated to the original momentum variable, implies

$$P_{2m}(k) = \frac{1}{m} + \mathcal{O}(k^{-1}) \quad \text{and} \quad P_{2m+1}(\eta) = \frac{2}{k} + \mathcal{O}(k^{-2}), \tag{4.7}$$

as $k \to \infty$. On the other hand, putting $\eta = -1 + \delta$ we get from (4.5) the following asymptotic expansion,

$$\lambda_n(\eta) = \begin{cases} 2i\delta \sum_{j=1}^{(d-2)/2} (-1)^{j+1}(d-2j)\sin\frac{2\pi nj}{d} + \mathcal{O}(\delta^2) & d \text{ even}, \\ 4i \sum_{j=1}^{(d-1)/2} (-1)^{j+1}\sin\frac{2\pi nj}{d} + \mathcal{O}(\delta) & d \text{ odd}, \end{cases} \tag{4.8}$$

where we used the fact that the members of the sum (4.5) appear in pairs having the same real parts while the imaginary ones differ by sign. Using next the fact that $\eta = -1 + 2k^{-1} + \mathcal{O}(k^{-2})$, we conclude from (4.3), (4.7), and (4.8) that $\mathcal{M}_d(k) = \mathcal{O}(k^{-1})$ holds as $k \to \infty$ for any natural $d \geq 3$. Note that the asymptotic behavior of both the prefactor and the eigenvalues depends on the vertex parity, however, the differences compensate mutually in the result. In the same way one can check that the violation measure $\mathcal{M}_d(k) = \mathcal{O}(k)$ as $k \to 0$.

For low values of d it is easy to evaluate the non-invariance measure explicitly. In particular, the eigenvalues (4.5) are $\{0, \pm\sqrt{3}i(1-\eta)\}$ and $\{0, 0, \pm 2i(1-\eta^2)\}$ for $d = 3, 4$, respectively, which yields

$$\mathcal{M}_3(k) = \frac{4k\sqrt{3}}{3+k^2} \quad \text{and} \quad \mathcal{M}_4(k) = \frac{4k}{1+k^2}. \tag{4.9}$$

As a concluding remark we note that (4.9) shows that $\mathcal{M}_3(k)$ saturates the unitarity bound $\mathcal{M}(k) \leq 2$ at $k = \sqrt{3}$, while $\mathcal{M}_4(k)$ does the same at $k = 1$.

V. THE FORM FACTOR

We focus in this section on the form factor, as given in (1.4). We change the point of view from the spectral statistics of the graph eigenvalues to those of the eigenphases of the corresponding unitary operator. This is a common practice within the spectral theory of quantum graphs (see Ref. 23 for justifications and proofs). Indeed, one observes that the eigenphase form factor follows the one of the eigenvalues (as demonstrated in Fig. 5, as well as in the other figures in this section). To be specific, denoting by E the number of graph edges, the form factor of the unitary operator is defined at the discrete times $\tau \in \frac{1}{2E}\mathbb{N}$ by (see, e.g., Ref. 8)

$$K_{\mathrm{U}}(\tau) = \frac{1}{2E}\lim_{\Lambda\to\infty}\frac{1}{2\Lambda}\int_{-\Lambda}^{\Lambda}\left|tr(\mathbf{U}(k))^{2E\tau}\right|^2 \mathrm{d}k, \tag{5.1}$$

where $\mathbf{U}(k)$ is a unitary $2E \times 2E$ matrix (often called the unitary evolution operator) given by

$$\mathbf{U}(k) = \exp(\mathrm{i}kL)\mathbf{S}(k),$$

with L being a diagonal matrix which stores the (directed) edge lengths and $\mathbf{S}(k)$ is the global scattering matrix of the graph. The matrix $\mathbf{S}(k)$ is comprised from the local vertex scattering matrices $S(k)$ [such as in (2.3)]. Note that we use bold font [as in $\mathbf{S}(k)$ and $\mathbf{U}(k)$] for matrices of dimensions $2E \times 2E$ defined on the whole graph, to be distinguished from the local vertex matrices S, U which are $d \times d$, where d is the degree of the vertex. Since the spectral statistics are dominated by the high energy asymptotics (see discussion in Sec. IV) we may replace the energy dependent scattering matrix $\mathbf{S}(k)$ with its high energy limit, which is comprised by the local vertex scattering matrices given in (4.2) (for an even degree vertex). Doing so, one sees that the only energy (k) dependence in (5.1) enters via the matrix $\exp(\mathrm{i}kL)$. Expanding $tr(\mathbf{U}(k))^{2E\tau}$ as a sum of products and performing the integral give the following useful expansion [see Ref. 8, Eq. (18)]:

$$K_{\mathrm{U}}(\tau) = \frac{1}{2E}\sum_{\mathrm{p},\mathrm{q}}\frac{(2E\tau)^2}{r_{\mathrm{p}}r_{\mathrm{q}}}A_{\mathrm{p}}A_{\mathrm{q}}^*\delta_{L_{\mathrm{p}},L_{\mathrm{q}}}, \tag{5.2}$$

where as above $2E\tau \in \mathbb{N}$. The sum in (5.2) is over pairs of periodic orbits consisting of $2E\tau$ edges and denoted by p, q. The total metric length of an orbit p is denoted by L_{p}, its overall scattering amplitude (which is a product of $\mathbf{S}$ entries corresponding to the orbit) is denoted by A_{p}. Furthermore, sometimes an orbit might be written as a repetition of a shorter orbit; in such a case the repetition number is denoted by r_{p} (if an orbit cannot be written as such repetition, then $r_{\mathrm{p}} = 1$). The expansion (5.2) is the starting point of the derivations in this section.

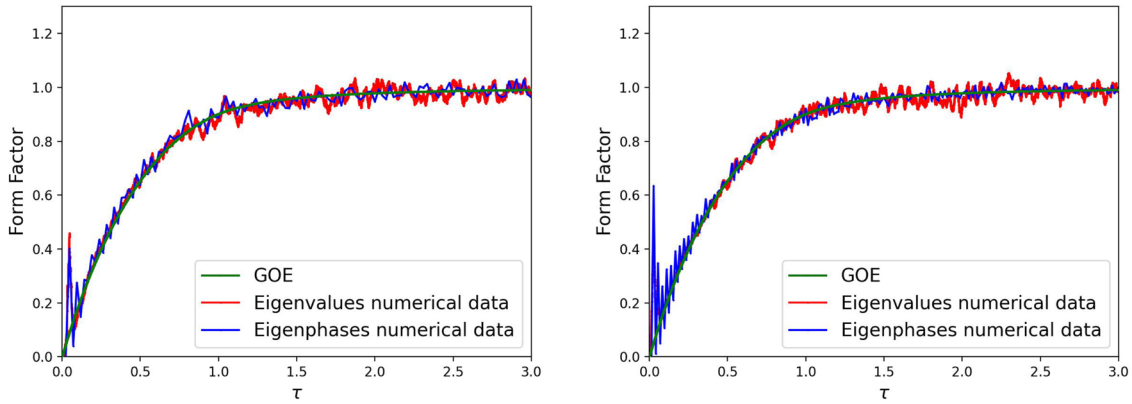

FIG. 5. The form factor of complete graphs (Left: K_7. Right: K_9). The curves correspond to: numerics of eigenvalues (red), numerics of the eigenphases (blue) and the theoretical GOE (green).

A. The form factor in the limit of infinite complete graphs

We consider here the infinite family of graphs, $\{K_V\}_{V\in 2\mathbb{N}+1}$, i.e., the family of complete graphs with an odd number of vertices. In general, in order to analytically prove any kind of RMT-like behaviour for graphs, one should consider families of increasing graphs (for finite graphs deviations might occur, as we indeed observe in this work). We choose here the particular family $\{K_V\}_{V\in 2\mathbb{N}+1}$ thanks to the somewhat easier book-keeping of the periodic orbits of complete graphs and since all of its vertices have even degrees (following the discussion in Sec. IV A). In the current subsection we calculate the leading term of the form factor in the limit of increasing graphs of this family; we verify that it is indeed the leading term of the GOE form factor [see (5.5)]. As a demonstration we provide in Fig. 5 the numerical calculation of the form factor for the graphs K_7 and K_9, two particular members of this graph family.

Consider a complete graph with V vertices and $E = \binom{V}{2}$ edges. As mentioned above, we take odd values of V and equip all vertices with preferred orientation conditions. Therefore in the high energy limit we get the vertex conditions as in (4.2), which we use in the following computation.

First, we classify the periodic orbits which are of a specific size n (namely, periodic orbits which consist of n edges). Each such orbit p has some $0 \le t \le n$ transmission scattering events and $n-t$ reflection scattering events; its overall scattering amplitude is therefore $A_{\mathrm{p}} = \pm\left(\frac{2}{V-1}\right)^t\left(1-\frac{2}{V-1}\right)^{n-t}$, since the degree of each vertex is $V-1$. The ambiguity in the $\pm$ sign is due to the term $(-1)^{i+j}$ in (4.2), when $i \neq j$ (i.e., transmission scattering event) and we show in the following that it does not affect the final result.

We claim that the number of such orbits (with t transmissions and $n-t$ reflections) is $\frac{2}{n}\binom{n}{t}\binom{V}{2}(V-2)^{t-2}$, assuming that $t \ge 2$; this combinatorial result is explained in the following. First, one picks the "starting" directed edge of the orbit, and there are $2E = 2\binom{V}{2}$ options for such a choice. Then, one chooses which of the n scattering events are the t transmissions, which gives the binomial factor $\binom{n}{t}$. When forming such an orbit, we know for each reflection event what is the next directed edge (it is just the last edge with a reversed direction); but for (almost) each transmission event we have $V-2$ possibilities to choose the next edge (it can be any edge emanating from the current vertex, apart from retracing along the last edge). Nevertheless, in this process, the two transmission events which appear after all other transmissions (but before some possible reflections) are uniquely determined in a way which ensures that the orbit returns back to the right "starting" edge. This gives a factor of $(V-2)^{t-2}$, noting that we assumed $t \ge 2$ (the case $t < 2$ is explained below). Then, we need to use a factor of $\frac{1}{n}$ since we consider periodic orbits up to cyclic shifts (and an orbits consists of n edges). Hence, multiplying all of the above we get a total number of $\frac{2}{n}\binom{n}{t}\binom{V}{2}(V-2)^{t-2}$ orbits which consist of t transmissions and $n-t$ reflections (counted up to cyclic shifts). To complement this computation we check the case $t < 2$. First, it is easy to see that there are no periodic orbits (on the complete graph) with only a single transmission ($t = 1$). Hence, we are left to deal with the orbits for which $t = 0$, meaning that they consist only of reflections and are supported on a single edge. Such orbits exist only for even values of n and their number is exactly the number of edges, $E = \binom{V}{2}$; their repetition number cannot be neglected, as it equals $r_{\mathrm{p}} = n/2$.

Now, we refer to (5.2) for the form factor computation. We consider $n = 2E\tau$, and next we will eventually take the limit of increasing graphs. Namely, $E \to \infty$ (or equivalently $V \to \infty$ in our case), while fixing the value of $\tau = \frac{2E}{n}$. When summing over pairs p, q of periodic orbits in (5.2) we need to take into account only orbits with the same metric lengths, i.e., $L_{\mathrm{p}} = L_{\mathrm{q}}$. Due to the complexity of this task, we do not consider all such pairs, but only pairs in which either $\mathrm{p} = \mathrm{q}$ or that p, q are the same up to a reversed direction (denoting this by $\mathrm{q} = \hat{\mathrm{p}}$). This is the well-known diagonal approximation and we will see that it successfully reproduces the leading term of the GOE form factor. Another common approximation that we implement here is to take $r_{\mathrm{p}} = r_{\mathrm{q}} = 1$ for almost all orbits, apart from the orbits for which we know their exact repetition number (these are the orbits with $t = 0$ and $r_{\mathrm{p}} = n/2$, already mentioned above). In the following computation we use the

shorthand notation $n := 2E\tau$, and return to the variable τ only at its end.

$$K_{\mathrm{diag}}(\tau) = \frac{n^2}{2E}\sum_{\mathrm{p}\,\mathrm{has}\,n\mathrm{edges}}\frac{1}{r_{\mathrm{p}}^2}\left(A_{\mathrm{p}}A_{\mathrm{p}}^* + A_{\mathrm{p}}A_{\hat{\mathrm{p}}}^*\right) = \frac{n^2}{E}\sum_{\mathrm{p}\,\mathrm{has}\,n\mathrm{edges}}\frac{1}{r_{\mathrm{p}}^2}A_{\mathrm{p}}A_{\mathrm{p}}^* = \frac{n^2}{E}\left[\frac{1}{2}\frac{1}{(n/2)^2}\binom{V}{2}\left(1-\frac{2}{V-1}\right)^{2n} + \sum_{t=2}^{n}\frac{2}{n}\binom{n}{t}\binom{V}{2}(V-2)^{t-2}\right.$$
$$\left.\times\left(\frac{2}{V-1}\right)^{2t}\left(1-\frac{2}{V-1}\right)^{2(n-t)}\right] = n^2\left[\frac{2}{n^2}\left(1-\frac{2}{V-1}\right)^{2n} + \sum_{t=2}^{n}\frac{2}{n}\binom{n}{t}(V-2)^{t-2}\left(\frac{2}{V-1}\right)^{2t}\left(1-\frac{2}{V-1}\right)^{2(n-t)}\right], \tag{5.3}$$

where in the above we used in the third line that for the first term ($t = 0$) the orbits are such that $\mathrm{p} = \hat{\mathrm{p}}$ and hence there should be introduced an additional factor of $1/2$, and in the last line we used $E = \binom{V}{2}$.

To continue the computation we note that a slight modification (starting from $t = 0$ rather than from $t = 2$) of the sum above gives

$$\sum_{t=0}^{n}\frac{2}{n}\binom{n}{t}(V-2)^{t-2}\left(\frac{2}{V-1}\right)^{2t}\left(1-\frac{2}{V-1}\right)^{2(n-t)} = \frac{2}{n}\frac{1}{(V-2)^2}\sum_{t=0}^{n}\binom{n}{t}(V-2)^{t}\left(\frac{2}{V-1}\right)^{2t}\left(1-\frac{2}{V-1}\right)^{2(n-t)}$$
$$= \frac{2}{n}\frac{1}{(V-2)^2}\left((V-2)\left(\frac{2}{V-1}\right)^2 + \left(1-\frac{2}{V-1}\right)^2\right)^n = \frac{2}{n(V-2)^2}.$$

We substitute this in (5.3), while subtracting the additional terms ($t = 0$ and $t = 1$), and get

$$K_{\mathrm{diag}}(\tau) = n^2\left[\frac{2}{n^2}\left(1-\frac{2}{V-1}\right)^{2n} + \frac{2}{n(V-2)^2} - \frac{2}{n}(V-2)^{-2}\left(1-\frac{2}{V-1}\right)^{2n} - 2(V-2)^{-1}\left(\frac{2}{V-1}\right)^2\left(1-\frac{2}{V-1}\right)^{2(n-1)}\right]$$
$$= \frac{2n}{(V-2)^2} + 2\left(1-\frac{2}{V-1}\right)^{2n}\left[1 - \frac{n}{(V-2)^2} - \frac{4n^2}{(V-1)^2(V-2)}\left(1-\frac{2}{V-1}\right)^{-2}\right] \underset{E\to\infty}{\longrightarrow} 2\tau, \tag{5.4}$$

where in the last line we used that $\tau = \frac{n}{2E}$ is fixed and since $E = \binom{V}{2}$, we get that $\frac{n}{V^2} \to \tau$ as $V \to \infty$. To see this, one can observe that the second term of the third line tends to $2\left(1-\frac{2}{V-1}\right)^{2\tau V^2}\left[1 - \tau - 4\tau^2 V\right]$, which goes to zero as $V \to \infty$.

We now see that for small values of τ, the calculation above indeed reproduces the first term of the GOE form factor:

$$K_{\mathrm{GOE}}(\tau) = \begin{cases} 2\tau - \tau\ln(1+2\tau) & \tau \le 1 \\ 2\tau - \tau\ln\left(\dfrac{2\tau+1}{2\tau-1}\right) & \tau \ge 1. \end{cases} \tag{5.5}$$

We note that the computation above is valid also for the Neumann-Kirchhoff conditions. This is because the scattering coefficients of the Neumann-Kirchhoff and of the asymptotic preferred orientation conditions are equal up to sign [see (4.2) and the text which follows it], but as we argued above, the sign is canceled in the diagonal approximation.

In the computation above, before taking the limit, we may examine the case $n = 2$ (so that $\tau = 1/E$). Returning to (5.3) and taking only the first term there (since $t = 0$ when $n = 2$), we get

$$K_{\mathrm{diag}}(1/E) = 2\left(1-\frac{2}{V-1}\right)^4. \tag{5.6}$$

This explains the peak which may be observed in Fig. 5 in the vicinity of zero and also explains why the peak for K_9 is higher than for K_7 (right and left parts of that figure). The expression (5.6) appeared already in [Ref. 61, Eq. (31)], where it is also explained that such orbits, which are repetitions of 2-edge orbits are responsible for the odd-even staggering phenomenon which ones obtains numerically for small values of τ.

B. The peak at half the Heisenberg time

We return to the observation made in the introduction - when numerically computing the form factor of the octahedron graph, we notice a clear and substantial (though local) deviation from GOE (Fig. 6, Left). Specifically, there is a clear peak which appears at half the Heisenberg time ($\tau = 1/2$). As far as we are aware of, such phenomenon was never observed in form factors of chaotic systems (to be accurate, a peak at $\tau = 1/2$ may be spotted in Ref. 51, Fig. 2, though there is no specific mention of this peak in the text). In what follows we explain the appearance of this peak and show that there are additional setups (other graphs and other vertex conditions) in which similar peaks appear. We start by considering a general graph Γ and upon need impose particular restrictions on the graph. We refer to the periodic orbit expansion (5.2) and employ it to evaluate the value $K_{\mathrm{U}}(1/2)$ and to show that it is substantially higher than its GOE prediction, $K_{\mathrm{GOE}}(1/2) = 1 - 1/2\ln(2)$.

Toward this we consider in the sum (5.2) only periodic orbits p, q which consist of $\frac{2E}{2} = E$ edges. Among such orbits we find the Eulerian cycles. An Eulerian cycle is a closed path on the graph which visits every edge of the graph exactly one time. For the sake of this definition we consider the undirected graph, i.e., every undirected edge appears exactly once in an Eulerian cycle. Therefore, the metric length of every Eulerian orbit equals the total length of the graph, which means in particular that $L_{\mathrm{p}} = L_{\mathrm{q}}$ for every pair of two Eulerian orbits, p, q and also

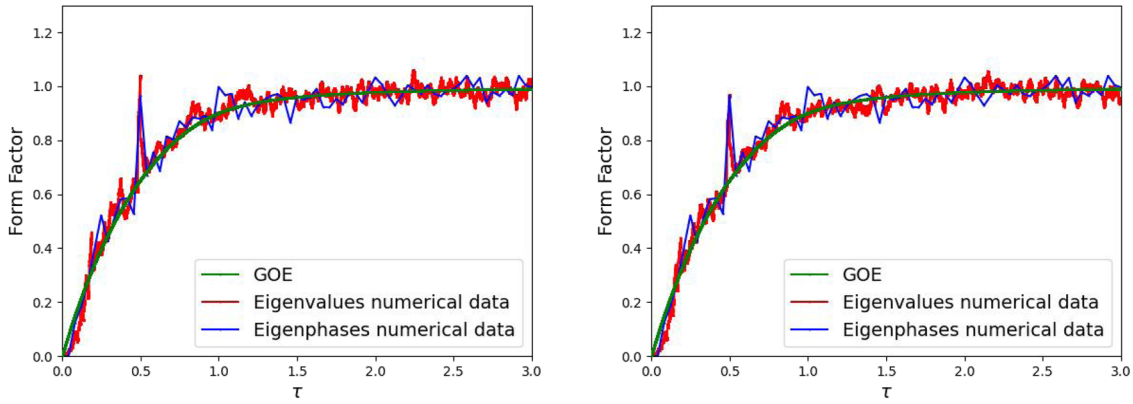

FIG. 6. The form factor of the octahedron graph. Left: with preferred orientation vertex conditions. Right: with Neumann-Kirchhoff vertex conditions. The curves correspond to: numerics of eigenvalues (red), numerics of the eigenphases (blue) and the theoretical GOE (green).

that $r_{\mathrm{p}} = r_{\mathrm{q}} = 1$. Therefore, the contribution of Eulerian cycles to the sum in (5.2) is given by $\frac{1}{2}E\sum_{\mathrm{p,q}\,\mathrm{Eulerian}} A_{\mathrm{p}}A_{\mathrm{q}}^{*}$. To calculate the amplitude A_{p} for an Eulerian cycle p, first observe that (by definition) all scattering events in an Eulerian cycle are transmissions. Therefore, by (4.2) we get $S_{i,j} = -\frac{2}{d}(-1)^{i+j}$ for any scattering event at any vertex. In addition, a vertex of even degree d is being visited exactly $d/2$ times throughout an Eulerian cycle, such that all edges connected to the vertex are eventually visited. Hence, for such a vertex the product of all $d/2$ scattering amplitudes (which are all transmissions) gives

$$\left(-\frac{2}{d}\right)^{d/2}\prod_{j=1}^{d}(-1)^{j} = \left(\frac{2}{d}\right)^{d/2},$$

where we used that the degree d is even and satisfies $d > 2$, and so both $d/2$ and the sum $\sum_{j=1}^{d} j$ are even. In order to simplify the following computations, we assume that the graph Γ is d-regular, i.e., all of its vertices are of degree d. In such a case, multiplying all the scattering amplitudes above for all the V vertices we get that $A_{\mathrm{p}} = \left(\frac{2}{d}\right)^{Vd/2} = \left(\frac{2}{d}\right)^{E}$ for each Eulerian orbit p. The relevant term in the form factor is therefore

$$\frac{1}{2}E\sum_{\mathrm{p,q}\,\mathrm{Eulerian}} A_{\mathrm{p}}A_{\mathrm{q}}^{*} = \frac{1}{2}E\left(\frac{2}{d}\right)^{2E}\left(\mathrm{N}_{\mathrm{Euler}}(\Gamma)\right)^{2}, \tag{5.7}$$

where $\mathrm{N}_{\mathrm{Euler}}(\Gamma)$ is the number of the Eulerian cycles of the graph Γ. To finish the computation we ought to count the number of Eulerian cycles of a graph, $\mathrm{N}_{\mathrm{Euler}}(\Gamma)$. This is a tedious task, which cannot be solved in a polynomial time for general undirected graphs. We elaborate more about this problem and its possible theoretical and practical resolutions in Subsection V C and in the Appendix.

If Γ is taken to be the octahedron graph then $\mathrm{N}_{\mathrm{Euler}}(\mathrm{Octahedron}) = 744$, which we obtained by running two independent algorithms (as detailed in Subsection V C and in the Appendix). To clarify, $\mathrm{N}_{\mathrm{Euler}}$ counts all the Eulerian orbits, where reversing the direction of an orbit is considered as a new orbit, but a cyclic shift of the orbit does not count as a new orbit. Substituting in (5.7) gives

$$\frac{1}{2}E\sum_{\mathrm{p,q}\,\mathrm{Eulerian}} A_{\mathrm{p}}A_{\mathrm{q}}^{*} \approx 0.198.$$

The GOE form factor is $K_{\mathrm{GOE}}(1/2) \approx 0.6534$, whereas the numerics gives $K_{\mathrm{U}}(1/2) \approx 0.9335 \pm 0.02$. Hence, the contribution of the Eulerian cycles explains slightly more than 70% of this mismatch. This is satisfying since in general the numerical values at $\tau = \frac{n}{2E}$ for even n are higher than the GOE prediction (and it is lower for odd values of n), which is due to the staggering phenomenon mentioned at the end of the previous subsection.

We note that the octahedron has many periodic orbits which consist of 12 edges; there are more than $1.4 \cdot 10^{6}$ of those. We get this number by computing $\frac{1}{12}tr\left(C^{12}\right) = 1398\,784$, where C is the 6×6 adjacency (connectivity) matrix of the octahedron graph. But, we take in consideration that computing via the trace of C^{12} underestimates the orbits p with repetition number $r_{\mathrm{p}} > 1$ (for those orbits we should divide the trace by $12/r_p$ and not by the global factor 12 as we do). Overall, we see that the number of Eulerian cycles is less than 0.05% from all the periodic orbits of size 12 (of the octahedron). Their substantial effect on the form factor is not because of their number, but it is thanks to the constructive interference between *every* two such periodic orbits. Namely, for the Eulerian cycles all the terms in the sum $\sum_{\mathrm{p,q}\,\mathrm{Eulerian}} A_{\mathrm{p}}A_{\mathrm{q}}^{*}$ are of positive sign and hence their contribution is constructive. This explains the dominance of the Eulerian cycles in this case and the dominance of the observed peak at $\tau = 1/2$.

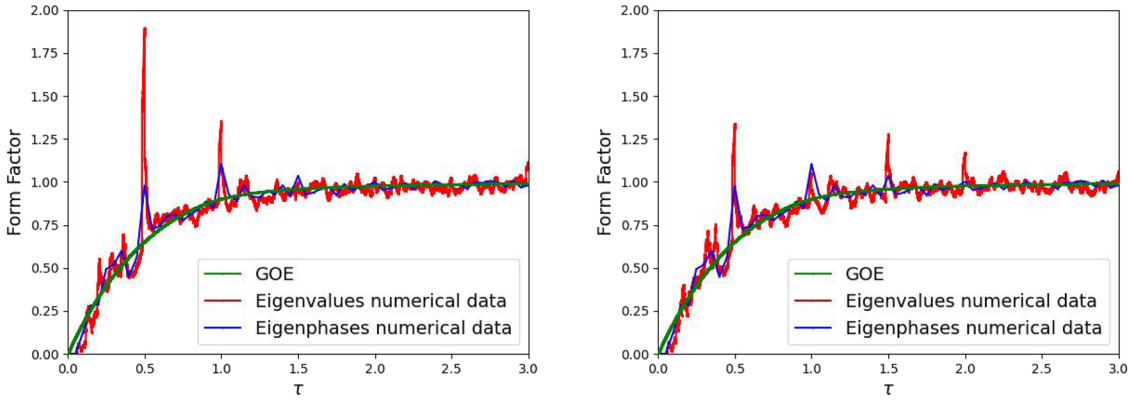

FIG. 7. The form factor of the K_5 graph. Numerics of eigenvalues (red), numerics of the eigenphases (blue) and the theoretical GOE (green). Left: with preferred orientation vertex conditions. Right: with Neumann-Kirchhoff vertex conditions.

We complement this computation by mentioning that changing the vertex conditions from preferred orientation to Neumann-Kirchhoff does not affect the result and the existence of the peak (see Fig. 6, Right). Indeed, the transmission amplitude of a scattering event for Neumann-Kirchhoff conditions is $2/d$, which equals the transmission coefficient in the preferred orientation conditions (this equality is up to sign which is always canceled in our case, as was already mentioned). Therefore the contribution of the Eulerian cycles computed in (5.7) is exactly the same if preferred orientation conditions are changed into Neumann-Kirchhoff.

Experimentally, we have observed the appearance of such a peak at $\tau = 1/2$ also for the complete graph K_5 (see Fig. 7). Repeating the computation above for K_5 gives

$$\frac{1}{2}E\sum_{\mathrm{p,q\ Eulerian}} A_{\mathrm{p}}A^{*}_{\mathrm{q}} = \frac{1}{2}E\left(\frac{2}{d}\right)^{2E}\left(\mathrm{N}_{\mathrm{Euler}}(K_5)\right)^2 \approx 0.332, \tag{5.8}$$

where we used that K_5 is a d-regular graph with $d = 4$, $E = 10$, and $\mathrm{N}_{\mathrm{Euler}}(K_5) = 264$. The computation in (5.8) agrees with the difference between the numerical (eigenphases) and the theoretical value, which is about 0.324.

Furthermore, we observe in the form factor for K_5 similar peaks at multiples of $\tau = 1/2$. A first attempt to explain those might be via orbits which are concatenation of a few Eulerian cycles (not necessarily a repetition of the same Eulerian cycle, but rather combining a few). But, such computations do not yield satisfactory values; the problem of providing a complete explanation for these particular peaks is still open.

We end this section by pointing out that the peak at $\tau = 1/2$ (and sometimes at its multiple) does not appear for every graph. For example, we do not see such peaks for graphs which are not Eulerian (i.e., they have no Eulerian cycles). A graph is Eulerian if and only if all of its vertices are of even degree; so complete graphs of the form K_{2n} are not Eulerian and indeed do not show these peaks. Nevertheless, even in the form factor of Eulerian graphs we do not necessarily see the aforementioned peaks. To give an example, this is the case with K_7 and K_9, as may be seen in Fig. 5. If we repeat the computation in (5.8) for K_7, substituting $E = 21$, $d = 6$ and $\mathrm{N}_{\mathrm{Euler}}(K_7) = 129\,976\,320$, we get that Eulerian cycles contribute 0.001 62 to the form factor at $\tau = 1/2$. This is indeed negligible comparing to the GOE value, $K_{\mathrm{GOE}}(1/2) \approx 0.6534$, so no peak is seen in this case.

Similarly, repeating the computation in (5.8) for K_9, substituting $E = 36$, $d = 8$ and $\mathrm{N}_{\mathrm{Euler}}(K_9) = 911\,520\,057\,021\,235\,200$, we get that Eulerian cycles contribute 6.7×10^{-7} to the form factor at $\tau = 1/2$, which is again negligible comparing to the GOE value.

We end by returning to the asymptotic computation of complete graphs from the previous subsection and checking whether the peak at $\tau = 1/2$ appears there. The asymptotic formula for the number of Eulerian cycles in complete graphs K_n (where n is odd and tends to infinity) is known to be (see Ref. 55),

$$\mathrm{N}_{\mathrm{Euler}}(K_n) = 2^{(n+1)/2}\pi^{1/2}\mathrm{e}^{-n^{12}/2+11/12}n^{(n-2)(n+1)/2}(1 + O(n^{-1/2+\epsilon})).$$

Using this asymptotics in (5.8) with $E = \binom{n}{2}$ and $d = n - 1$ gives that the contribution to the form factor is of order

$$2^{(2n^2-n-3)/2}\pi^{1/2}\mathrm{e}^{-n^{12}/2+11/12}n^{-(n-3)(n+2)/2}(1 + O(n^{-1/2+\epsilon})),$$

which converges to 0, as n tends to infinity.

C. The problem of counting Eulerian cycles

The general problem of counting the exact number of Eulerian cycles of an *undirected* graph belongs to the class of #p-complete problems.[22] This means in particular that there is no known polynomial time algorithm which solves it. Furthermore, if such polynomial solution

is found it would imply that all #*p* problems could also be solved in polynomial time, which would lead to significant implications in computational complexity theory. (These are analogous to *NP* problems, but instead of just finding whether a solution to the problem exists, one is required to counting the number of all the possible solutions.) We do not aim here to cover the background on this computational problem and merely mention a very recent preprint which offers a new approach and reviews the existing literature.[54] The problem of counting periodic orbits and even estimating their number or providing asymptotics plays an important role in quantum chaos, as it allows a better control when using trace formulae for the study of spectral statistics. The orbit counting problem is relevant for graphs, as well as for the case of symbolic dynamics. In both cases one wishes to cluster the periodic orbits according to the relevant problem. For example, in the case of metric graphs one would like to cluster all orbits according to their support. Such a cluster would contain all orbits, which share the number of times they transverse each of the graph edges. Using this approach and offering numerical as well as analytical solutions to it was done in Refs. 8, 28, 37, 51, 61, 62, and 64 for specific families of metric graphs and in Refs. 34 and 35 for general systems, by considering symbolic dynamics.

We mention here two different algorithms which we have used in order to exactly count the number of Eulerian cycles in the graphs considered in this paper.

First, we note that in the case of a directed graph there is a well-known polynomial time algorithm to count the number of Eulerian cycles. This algorithm is based on the BEST theorem (after de Bruijn, van Aardenne-Ehrenfest, Smith, and Tutte) which provides an explicit formula for the number of Eulerian cycles in terms of the number of spanning trees of a graph.[63,66] One may apply such an algorithm straightforwardly to our problem (i.e., counting for non-directed graphs): enumerate over all possible assignments of directions of edges and for each perform the BEST algorithm. This is clearly exponential in the number of graph edges due to the enumeration, but may still be performed for small enough graphs. Indeed, we used this for the computation of the N_{Euler} values given in the previous subsection.

The other algorithm we have used is new, to the best of our knowledge, and we describe it in detail in Appendix. Both algorithms are of similar order of complexity, but the algorithm provided in the appendix may be used to count other families of periodic orbits beyond Eulerian cycles and also to evaluate their contribution to the spectral statistics.

ACKNOWLEDGMENTS

We greatly benefited from interesting discussions with Gregory Berkolaiko and Uzy Smilansky on random matrix theory in the context of quantum graphs. We had stimulating discussions with Sven Gnutzmann, Boris Gutkin and Holger Schanz about periodic orbit expansions. We thank all of them for enriching our knowledge on these topics. Special thanks are due to Jon Harrison for his thoughtful feedback on this manuscript.

R.B. was supported by the Israel Science Foundation (ISF Grant No. 844/19) and by the Binational Foundation Grant (Grant No. 2016281). P.E. was partially supported by the European Union's Horizon 2020 research and innovation programme under the Marie Skłodowska-Curie Grant Agreement No. 873071.

AUTHOR DECLARATIONS

Conflict of Interest

The authors have no conflicts to disclose.

Author Contributions

Ram Band: Investigation (equal); Writing – original draft (lead); Writing – review & editing (lead). **Pavel Exner**: Investigation (equal); Writing – original draft (equal); Writing – review & editing (equal). **Divya Goel**: Data curation (equal); Investigation (equal). **Aviya Strauss**: Data curation (equal); Investigation (equal).

DATA AVAILABILITY

The data that support the findings of this study are available from the corresponding author upon reasonable request.

APPENDIX: AN ALGORITHM FOR COUNTING PERIODIC ORBITS

We present here a procedure for counting families periodic orbits. We applied it numerically for the counting of Eulerian cycles which play important role in the current work. Nevertheless, this scheme may be applied for counting various types of orbits.

1. The adjacency matrix for orbit counting

Let Γ be a directed graph with the vertex set $\mathcal{V}$ and the directed edge set $\mathcal{E}$. We consider here edge sets with the property $e \in \mathcal{E} \Leftrightarrow \hat{e} \in \mathcal{E}$, where $\hat{e}$ denotes the reverse direction of an edge e. As a starting point for counting periodic orbits we use the graph adjacency matrix $A(\Gamma)$,

which is a $V \times V$ matrix such that

$$[A(\Gamma)]_{i,j} = \begin{cases} 1 & (j,i) \text{is a directed edge} \\ 0 & \text{otherwise} \end{cases}, \tag{A1}$$

where we assume that two vertices may be connected by at most a single edge. Because every directed edge also appears with its reverse direction, we get that the matrix A is symmetric, $A_{i,j} = A_{j,i}$. Observe that the number of periodic orbits of length n of the graph is characterized by $tr(A^n)$. Here, one should be careful because some orbits are counted with multiplicity. Specifically, the periodic orbits are counted in $tr(A^n)$ with some factor which is due to taking cyclic permutations. Namely, a certain orbit $(v_1, v_2, \ldots, v_n, v_1)$ with all vertices different $v_i \neq v_j$ will be counted n times in $tr(A^n)$, since all its cyclic permutations $(v_k, v_{k+1}, \ldots, v_n, v_1, v_2, \ldots, v_k)$, for $1 \leq k \leq n$, will be counted. There are particular orbits which are repetitions of shorter orbits, such as $\mathrm{p} = (v_1, v_2, \ldots, v_m, v_1, v_2, \ldots, v_m, \ldots, v_1, v_2, \ldots, v_m)$. Here we assume as before that $v_i \neq v_j$ for $1 \leq i, j \leq m$ and that repeated vertices are indicated explicitly. In such a case we get that $m \mid n$ (i.e., m divides n) and further denote $r_{\mathrm{p}} := \frac{n}{m}$, which is called the repetition number of the orbit p. Using this notation, we see that each periodic orbit of length n is counted exactly n/r_{p} times in $tr(A^n)$. We summarize this by writing

$$tr(A^n) = \sum_{\mathrm{p} \in \mathcal{PO}_n} \frac{n}{r_{\mathrm{p}}} = n \sum_{\mathrm{p} \in \mathcal{PO}_n} \frac{1}{r_p}, \tag{A2}$$

where $\mathcal{PO}_n$ is the set of periodic orbits of length n, and r_{p} is the repetition number of the orbit p.

2. Counting orbits of subgraphs

Next, we wish to count the orbits of subgraphs of Γ. To do so, we repeat exactly the same arguments of the previous subsection, but for a modified adjacency matrix. Explicitly, let $\widetilde{\Gamma}$ be a subgraph of Γ having the same vertex set $\mathcal{V}$ as Γ, but only a subset of the directed edges $\widetilde{\mathcal{E}} \subset \mathcal{E}$ (for example, in this subset it might happen that a certain edge appears but its reverse does not). We construct the adjacency matrix $A(\widetilde{\Gamma})$ of the subgraph as a $V \times V$ matrix such that

$$\left[A(\widetilde{\Gamma})\right]_{i,j} = \begin{cases} 1 & (j,i) \in \widetilde{\mathcal{E}} \\ 0 & \text{otherwise} \end{cases}.$$

We still have that the analogue of (A2) holds, but obviously in the sum on the right hand side only periodic orbits which are supported on the edges set $\widetilde{\mathcal{E}}$ are taken into account.

3. Introducing vectors of counts

We introduce the following notation for the power set of the edge set, $\mathcal{B} := \mathbb{Z}_2^{|\mathcal{E}|}$. With this notation there is a bijection between subsets $\widetilde{\mathcal{E}} \subset \mathcal{E}$ and $\underline{b} \in \mathcal{B}$, and we may think of the latter as sequences of bits of length $|\mathcal{E}|$. From now on, we fix n (the length of the periodic orbits we are counting) and denote

$$\widetilde{N}_{\underline{b}} := tr\left(A(\widetilde{\Gamma})^n\right), \tag{A3}$$

where $\underline{b} \in \mathcal{B}$ corresponds to the edge subset $\widetilde{\mathcal{E}}$ of the subgraph $\widetilde{\Gamma}$. We note that $\widetilde{N}_{\underline{b}}$ counts the periodic orbits whose support is $\underline{b}$ or a subset of $\underline{b}$ is understood from now on as an edge subset).

We denote by $\mathrm{supp}(\mathrm{p})$ the subset of edges which the periodic orbit p contains, and allow ourselves to write $\mathrm{supp}(\mathrm{p}) \in \mathcal{B}$, thanks to the bijection between $\mathcal{B}$ and edge subsets. It might be that a certain edge appears more than once in p, but such information is not reflected in the notation $\mathrm{supp}(\mathrm{p})$.

With that notation we write [following (A2)],

$$\widetilde{N}_{\underline{b}} = n \sum_{\mathrm{supp}(p) \subseteq \underline{b}} \frac{1}{r_{\mathrm{p}}}, \tag{A4}$$

and

$$N_{\underline{b}} := n \sum_{\mathrm{supp}(p) = \underline{b}} \frac{1}{r_{\mathrm{p}}}, \tag{A5}$$

where we sum only over $\mathrm{p} \in \mathcal{PO}_n$, and noting that the difference between $\widetilde{N}_{\underline{b}}$ and $N_{\underline{b}}$ is whether the considered periodic orbits are supported exactly on $\underline{b}$ or on some subset of it.

We consider the vectors $\left(\widetilde{N}_{\underline{b}}\right)_{\underline{b} \in \mathcal{B}}$ and $\left(N_{\underline{b}}\right)_{\underline{b} \in \mathcal{B}}$ as vectors of lengths $2^{|\mathcal{E}|}$. Namely, $\widetilde{N}, N \in \mathbb{N}_0^{2^{|\mathcal{E}|}}$, where $\mathbb{N}_0 := \mathbb{N} \cup \{0\}$.

The vector $\left(N_{\underline{b}}\right)_{\underline{b} \in \mathcal{B}}$ may be used to count various families of periodic orbits. As an example, we demonstrate how it can be used to count Eulerian cycles. We start by observing that there are necessary conditions which a certain $\underline{b} \in \mathcal{B}$ must fulfill in order to be the support of an

Eulerian cycle. Namely, $\underline{b}$ should correspond to a subset $\widetilde{\mathcal{E}} \subset \mathcal{E}$ which contains exactly $|\mathcal{E}|/2$ edges and satisfies $e \in \widetilde{\mathcal{E}} \Leftrightarrow \hat{e} \notin \widetilde{\mathcal{E}}$ (but this is not a sufficient condition). We denote the set of these admissible $\underline{b}$ values by $\mathcal{B}_{\text{Euler}}$. Using this, the number of Eulerian cycles of the graph Γ is

$$\mathrm{N}_{\text{Euler}}(\Gamma) = \frac{2}{|\mathcal{E}|} \sum_{\underline{b} \in \mathcal{B}_{\text{Euler}}} N_{\underline{b}}, \tag{A6}$$

where we used (A5) and that $n = |\mathcal{E}|/2$ and that $r_{\mathfrak{p}} = 1$ for an Eulerian cycle $\mathfrak{p}$.

Next, we describe how to express the vector $\left(N_{\underline{b}}\right)_{\underline{b} \in \mathcal{B}}$ in terms of the vector $\left(\widetilde{N}_{\underline{b}}\right)_{\underline{b} \in \mathcal{B}}$. The latter vector was already explicitly expressed in (A3).

4. Transform from $\widetilde{N}_{\underline{b}}$ to $N_{\underline{b}}$

We keep in mind that $1 \le n \le |\mathcal{E}|$ is fixed throughout the section (for Eulerian cycles one takes $n = |\mathcal{E}|/2$, but we continue describing the scheme for an arbitrary value of n). By definition and from (A4) and (A5), one observes that the values $\left(N_{\underline{b}}\right)_{\underline{b} \in \mathcal{B}}$ may be expressed in terms of $\left(\widetilde{N}_{\underline{b}}\right)_{\underline{b} \in \mathcal{B}}$ by using the inclusion–exclusion principle. To write this, we introduce a few additional notations. Denote by $\mathrm{popcnt}(\underline{b})$ the number of 1's which $\underline{b}$ contains. Furthermore, if $\widetilde{\underline{b}}, \widehat{\underline{b}} \in \mathcal{B}$ correspond to some edge subsets $\widetilde{\mathcal{E}}, \widehat{\mathcal{E}} \subset \mathcal{E}$ then we denote $\widetilde{\underline{b}} \subset \widehat{\underline{b}}$ iff $\widetilde{\mathcal{E}} \subset \widehat{\mathcal{E}}$. We further emphasize this by writing that $\widetilde{\underline{b}} \subset \widehat{\underline{b}}$ iff $\widetilde{\underline{b}} \& \widehat{\underline{b}} = \widetilde{\underline{b}}$, where notation & is the pair-wise 'AND' operation between bits. Given $\underline{b} \in \mathcal{B}$ we denote for all $k \in \mathbb{N}$,

$$\mathcal{B}_{\underline{b}}(k) := \left\{\widetilde{\underline{b}} \in \mathcal{B} : \widetilde{\underline{b}} \subset \underline{b} \text{ and } \mathrm{popcnt}(\widetilde{\underline{b}}) = \mathrm{popcnt}(\underline{b}) - k\right\}.$$

Using these notation we employ the inclusion–exclusion principle and get

$$N_{\underline{b}} = \widetilde{N}_{\underline{b}} - \sum_{\widetilde{\underline{b}} \in \mathcal{B}_{\underline{b}}(1)} \widetilde{N}_{\widetilde{\underline{b}}} + \sum_{\widetilde{\underline{b}} \in \mathcal{B}_{\underline{b}}(2)} \widetilde{N}_{\widetilde{\underline{b}}} - \cdots + (-1)^{n-1} \sum_{\widetilde{\underline{b}} \in \mathcal{B}_{\underline{b}}(n-1)} \widetilde{N}_{\widetilde{\underline{b}}} + (-1)^{n} \sum_{\widetilde{\underline{b}} \in \mathcal{B}_{\underline{b}}(n)} \widetilde{N}_{\widetilde{\underline{b}}}, \tag{A7}$$

where we use that $\mathrm{popcnt}(\underline{b}) \le n$. Note also that $\mathcal{B}_{\underline{b}}(k) = \emptyset$ for $k > \mathrm{popcnt}(\underline{b})$ and $\mathcal{B}_{\underline{b}}(\mathrm{popcnt}(\underline{b})) = \{(0, \ldots, 0)\}$ and $\widetilde{N}_{(0,\ldots,0)} = 0$; which means in particular that the last summand in (A7) always vanishes $(-1)^n \sum_{\widetilde{\underline{b}} \in \mathcal{B}_{\underline{b}}(n)} \widetilde{N}_{\widetilde{\underline{b}}} = 0$.

Let us consider $\left(N_{\underline{b}}\right)_{\underline{b} \in \mathcal{B}}$ and $\left(\widetilde{N}_{\underline{b}}\right)_{\underline{b} \in \mathcal{B}}$ as vectors in $\mathbb{R}^{\mathcal{B}}$, recalling that $|\mathcal{B}| = 2^{|\mathcal{E}|}$. Equation (A7) presents the vector $\left(N_{\underline{b}}\right)_{\underline{b} \in \mathcal{B}}$ as a linear transform of the vector $\left(\widetilde{N}_{\underline{b}}\right)_{\underline{b} \in \mathcal{B}}$. Denoting the matrix representing this linear transformation by $Y_{|\mathcal{E}|}$, we see that its entries are 0, ±1 and furthermore it has a recursive representation as

$$\begin{aligned} Y_1 &:= \begin{pmatrix} 1 & 0 \\ -1 & 1 \end{pmatrix}, \\ Y_n &= Y_1 \otimes Y_{n-1}, \quad \forall n > 1, \end{aligned} \tag{A8}$$

where $\otimes$ denotes the Kronecker product of matrices. This transform is also known as the arithmetic transform, which is closely related to the well-known Walsh-Hadamard transform.[4]

This special form of the matrices allows an efficient algorithm which multiplies the matrix $Y_{|\mathcal{E}|}$ with the vector $\left(\widetilde{N}_{\underline{b}}\right)_{\underline{b} \in \mathcal{B}}$ to obtain the vector $\left(N_{\underline{b}}\right)_{\underline{b} \in \mathcal{B}}$. This algorithm uses a method similar to the fast Walsh-Hadamard. Its complexity is $|\mathcal{B}| \log(|\mathcal{B}|) = |\mathcal{E}| 2^{|\mathcal{E}|}$ instead of the usual complexity of multiplying a matrix by a vector (which is $|\mathcal{B}|^2 = 2^{2|\mathcal{E}|}$ in our case).

5. Algorithmic summary and complexity

We summarize the steps of the algorithm described above for computing $\mathrm{N}_{\text{Euler}}(\Gamma)$ and its overall complexity:

(1) Preparing the vector $\left(\widetilde{N}_{\underline{b}}\right)_{\underline{b} \in \mathcal{B}}$, as in (A3). We need to perform $|\mathcal{B}| = 2^{|\mathcal{E}|}$ times the computation $tr\left(A(\widetilde{\Gamma})^{|\mathcal{E}|/2}\right)$ (with a different subgraph $\widetilde{\Gamma}$ every time). Overall the complexity is $O\left(2^{|\mathcal{E}|} |\mathcal{V}|^k \log|\mathcal{E}|\right)$, with $2.37 \lesssim k \le 3$ (k depends on the multiplication algorithm we choose, see e.g., Ref. 1).

(2) Transforming $\left(\widetilde{N}_{\underline{b}}\right)_{\underline{b} \in \mathcal{B}}$ into $\left(N_{\underline{b}}\right)_{\underline{b} \in \mathcal{B}}$ using the arithmetic transform given by (A8). The complexity is $O(|\mathcal{B}| \log(|\mathcal{B}|)) = O\left(|\mathcal{E}| 2^{|\mathcal{E}|}\right)$.

(3) Summing the relevant entries of $\left(N_{\underline{b}}\right)_{\underline{b} \in \mathcal{B}}$, see (A6). Overall it means to sum $|\mathcal{B}_{\text{Euler}}| = 2^{|\mathcal{E}|/2}$ entries.The total complexity is hence $O\left(2^{|\mathcal{E}|}\left(|\mathcal{E}| + |\mathcal{V}|^k \log|\mathcal{E}|\right)\right)$ with $2.37 \lesssim k \le 3$ (depending on the multiplication algorithm).

6. Concluding remarks and variations on the algorithm

A first variation on the scheme described above would be to replace the adjacency matrix A in (A1) by the overall $|\mathcal{E}| \times |\mathcal{E}|$ scattering matrix, $\mathbf{S}$ or some modifications of it. For example, we may use an $|\mathcal{E}| \times |\mathcal{E}|$ matrix $\mathbf{M}$, defined by $\mathbf{M}_{i,j} = \mathbf{S}_{i,j}^2$ to evaluate the diagonal approximation as in (5.3). Specifically, one may take the analogue of (A3) to define $\widetilde{N}_{\underline{b}} := tr\left(\mathbf{M}(\widetilde{\Gamma})^n\right)$. Transforming $\widetilde{N}_{\underline{b}}$ (by the same arithmetic transform) gives the vector $N_{\underline{b}}$, the sum of whose entries is the corresponding value of the diagonal approximation.

Another variation of the algorithm is relevant for its implementation. Rather then fixing a single value of n and raising all matrices to this power n, one may take several such n values and correspondingly prepare several vectors $\left(\widetilde{N}_{\underline{b}}\right)_{\underline{b} \in \mathcal{B}}$ (one for each power n). Then the arithmetic transform to turn them into $\left(N_{\underline{b}}\right)_{\underline{b} \in \mathcal{B}}$ may be done in parallel, thus making the computation more efficient.

REFERENCES

[1] Ambainis, A., Filmus, Y., and Le Gall, F., "Fast matrix multiplication: Limitations of the laser method," in *Proceedings of the 47th Annual ACM Symposium on Theory of Computing (STOC)* (2015), pp. 585–593.
[2] Akila, M. and Gutkin, B., "Spectral statistics of nearly unidirectional quantum graphs," J. Phys. Math. Theor. **48**(34), 345101 (2015).
[3] Akila, M. and Gutkin, B., "GSE spectra in uni-directional quantum systems," J. Phys. Math. Theor. **52**(23), 235201 (2019).
[4] Arndt, J., *The Walsh Transform and Its Relatives* (Springer Berlin Heidelberg, Berlin, Heidelberg, 2011), pp. 459–496.
[5] Bolte, J. and Endres, S., "The trace formula for quantum graphs with general self adjoint boundary conditions," Ann. Henri Poincare **10**(1), 189–223 (2009).
[6] Berkolaiko, G., "Quantum Star Graphs and Related Systems," Ph.D. thesis, University of Bristol, 2000.
[7] Berkolaiko, G., "Form factor for large quantum graphs: Evaluating orbits with time reversal," Waves Random Media **14**(1), S7–S27 (2004).
[8] Berkolaiko, G., "Form factor expansion for large graphs: A diagrammatic approach," in *Quantum Graphs and Their Applications*, *Contemporary Mathematics Vol. 415* (American Mathematical Society, Providence, RI, 2006), pp. 35–49.
[9] Berkolaiko, G., "An elementary introduction to quantum graphs," in *Geometric and Computational Spectral Theory*, *Contemporary Mathematics Vol. 700* (American Mathematical Society, Providence, RI, 2017), pp. 41–72.
[10] Barra, F. and Gaspard, P., "On the level spacing distribution in quantum graphs," J. Stat. Phys. **101**(1–2), 283–319 (2000).
[11] Band, R. and Gnutzmann, S., "Quantum graphs via exercises," in *Spectral Theory and Applications*, *Contemporary Mathematics Vol. 720* (American Mathematical Society, Providence, RI, 2018), pp. 187–203.
[12] Bohigas, O., Giannoni, M. J., and Schmit, C., "Characterization of chaotic quantum spectra and universality of level fluctuation laws," Phys. Rev. Lett. **52**(1), 1–4 (1984).
[13] Bolte, J. and Harrison, J., "Spectral statistics for the Dirac operator on graphs," J. Phys. Math. Gen. **36**(11), 2747–2769 (2003).
[14] Bolte, J. and Harrison, J., "The spin contribution to the form factor of quantum graphs," J. Phys. Math. Gen. **36**(27), L433–L440 (2003).
[15] Bolte, J. and Harrison, J., "The spectral form factor for quantum graphs with spin-orbit coupling," in *Quantum Graphs and Their Applications*, *Contemporary Mathematics Vol. 415* (American Mathematical Society, Providence, RI, 2006), pp. 51–64.
[16] Band, R., Harrison, J. M., and Joyner, C. H., "Finite pseudo orbit expansions for spectral quantities of quantum graphs," J. Phys. Math. Theor. **45**(32), 325204 (2012).
[17] Band, R., Harrison, J. M., and Sepanski, M., "Lyndon word decompositions and pseudo orbits on q-nary graphs," J. Math. Anal. Appl. **470**(1), 135–144 (2019).
[18] Berkolaiko, G. and Keating, J. P., "Two-point spectral correlations for star graphs," J. Phys. Math. Gen. **32**(45), 7827–7841 (1999).
[19] Berkolaiko, G. and Kuchment, P., *Introduction to Quantum Graphs*, *Mathematical Surveys and Monographs Vol. 186* (AMS, 2013).
[20] Berkolaiko, G., Schanz, H., and Whitney, R. S., "Leading off-diagonal correction to the form factor of large graphs," Phys. Rev. Lett. **88**, 104101 (2002).
[21] Berkolaiko, G., Schanz, H., and Whitney, R. S., "Form factor for a family of quantum graphs: An expansion to third order," J. Phys. Math. Gen. **36**(31), 8373–8392 (2003).
[22] G. R. Brightwell and P. Winkler, "Counting Eulerian circuits is #p-complete," in *ALENEX/ANALCO* (2005).
[23] Berkolaiko, G. and Winn, B., "Relationship between scattering matrix and spectrum of quantum graphs," Trans. Am. Math. Soc. **362**(12), 6261–6277 (2010).
[24] Che, J., Gluth, N., Köhnes, S., Guhr, T., and Dietz, B., "Experimental study of the distributions of off-diagonal scattering-matrix elements of quantum graphs with symplectic symmetry," arXiv:2505.09573 (2025).
[25] Davis, P. J., *Circulant Matrices*, *Pure and Applied Mathematics* (A Wiley-Interscience Publication and John Wiley & Sons, New York, Chichester, Brisbane, 1979).
[26] Dietz, B., Klaus, T., Masi, M., Miski-Oglu, M., Richter, A., Skipa, T., and Wunderle, M., "Closed and open superconducting microwave waveguide networks as a model for quantum graphs," Phys. Rev. E **109**, 034201 (2024).
[27] Dietz, B., Yunko, V., Białous, M., Bauch, S., Ławniczak, M., and Sirko, L., "Nonuniversality in the spectral properties of time-reversal-invariant microwave networks and quantum graphs," Phys. Rev. E **95**, 052202 (2017).
[28] Echols, I., Harrison, J., and Hudgins, T., "Periodic orbits on 2-regular circulant digraphs," Graphs Comb. **41**(3), 67 (2025).
[29] Exner, P. and Tater, M., "Quantum graphs with vertices of a preferred orientation," Phys. Lett. **382**(5), 283–287 (2018).
[30] Exner, P. and Tater, M., "Quantum graphs: Self-adjoint, and yet exhibiting a nontrivial *PT*-symmetry," Phys. Lett. **416**(6), 127669 (2021).
[31] Farooq, O., Akhshani, A., Ławniczak, M., Białous, M., and Sirko, L., "Coupled unidirectional chaotic microwave graphs," Phys. Rev. E **110**, 014206 (2024).
[32] Gnutzmann, S. and Altland, A., "Universal spectral statistics in quantum graphs," Phys. Rev. Lett. **93**, 194101 (2004).
[33] Gnutzmann, S. and Altland, A., "Spectral correlations of individual quantum graphs," Phys. Rev. E **72**(5), 056215 (2005).
[34] Gutkin, B. and Osipov, V., "Clustering of periodic orbits and ensembles of truncated unitary matrices," J. Stat. Phys. **153**(6), 1049–1064 (2013).
[35] Gutkin, B. and Al Osipov, V., "Clustering of periodic orbits in chaotic systems," Nonlinearity **26**(1), 177–200 (2013).
[36] Gnutzmann, S. and Smilansky, U., "Quantum graphs: Applications to quantum chaos and universal spectral statistics," Adv. Phys. **55**(5–6), 527–625 (2006).
[37] Gavish, U. and Smilansky, U., "Degeneracies in the length spectra of metric graphs," J. Phys. Math. Theor. **40**(33), 10009–10020 (2007).
[38] Gnutzmann, S. and Smilansky, U., "Information scrambling and chaos induced by a Hermitian matrix," J. Phys. Math. Theor. **57**(37), 37LT01 (2024).
[39] Hul, O., Bauch, S., Pakoński, P., Savytskyy, N., Życzkowski, K., and Sirko, L., "Experimental simulation of quantum graphs by microwave networks," Phys. Rev. E **69**, 056205 (2004).

[40]Harrison, J. M. and Hudgins, T., "Complete dynamical evaluation of the characteristic polynomial of binary quantum graphs," J. Phys. Math. Theor. **55**(42), 425202 (2022).
[41]Harrison, J. M. and Hudgins, T., "Periodic orbit evaluation of a spectral statistic of quantum graphs without the semiclassical limit," Europhys. Lett. **138**(3), 30002 (2022).
[42]Hofmann, T., Lu, J., Kuhl, U., and Stöckmann, H.-J., "Spectral duality in graphs and microwave networks," Phys. Rev. E **104**, 045211 (2021).
[43]Hul, O. and Sirko, L., "Parameter-dependent spectral statistics of chaotic quantum graphs: Neumann versus circular orthogonal ensemble boundary conditions," Phys. Rev. E **83**, 066204 (2011).
[44]Harrison, J. M. and Swindle, E., "Spectral properties of quantum circulant graphs," J. Phys. Math. Theor. **52**(28), 285101 (2019).
[45]Harrison, J. M. and Winn, B., "Intermediate statistics for a system with symplectic symmetry: The Dirac rose graph," J. Phys. Math. Theor. **45**(43), 435101 (2012).
[46]Joyner, C. H., Müller, S., and Sieber, M., "GSE statistics without spin," Europhys. Lett. **107**(5), 50004 (2014).
[47]Kostenko, A. and Nicolussi, N., *Laplacians on Infinite Graphs*, *Memoirs of the European Mathematical Society Vol. 3* (EMS Press, Berlin, 2022; 2023).
[48]Kottos, T. and Smilansky, U., "Quantum chaos on graphs," Phys. Rev. Lett. **79**(24), 4794–4797 (1997).
[49]Kostrykin, V. and Schrader, R., "Kirchhoff's rule for quantum wires," J. Phys. Math. Gen. **32**(4), 595–630 (1999).
[50]Kottos, T. and Smilansky, U., "Periodic orbit theory and spectral statistics for quantum graphs," Ann. Phys. **274**(1), 76–124 (1999).
[51]Kottos, T. and Schanz, H., "Quantum graphs: A model for quantum chaos," Physica E **9**(3), 523–530 (2001), part of Special Issue: Proceedings of an International Workshop and Seminar on the Dynamics of Complex Systems.
[52]Kurasov, P., *Spectral Geometry of Graphs*, *Operator Theory: Advances and Applications Vol. 293* (Birkhäuser/Springer, Berlin, 2024).
[53]Lu, J., Hofmann, T., Kuhl, U., and Stöckmann, H.-J., "Implications of spectral interlacing for quantum graphs," Entropy **25**(1), 109 (2023).
[54]Luo, Y., "On a trace formula of counting Eulerian cycles," arXiv:2502.02915 (2025).
[55]McKay, B. D. and Robinson, R. W., "Asymptotic enumeration of Eulerian circuits in the complete graph," Comb. Probab. Comput. **7**(4), 437 (1998).
[56]Pluhař, Z. and Weidenmüller, H. A., "Universal chaotic scattering on quantum graphs," Phys. Rev. Lett. **110**, 034101 (2013).
[57]Pluhař, Z. and Weidenmüller, H. A., "Universal quantum graphs," Phys. Rev. Lett. **112**, 144102 (2014).
[58]Pluhař, Z. and Weidenmüller, H. A., "Quantum graphs and random-matrix theory," J. Phys. A **48**(27), 275102 (2015).
[59]Rehemanjiang, A., Allgaier, M., Joyner, C. H., Müller, S., Sieber, M., Kuhl, U., and Stöckmann, H.-J., "Microwave realization of the Gaussian symplectic ensemble," Phys. Rev. Lett. **117**, 064101 (2016).
[60]Rofe-Beketov, F. S., "Selfadjoint extensions of differential operators in a space of vector-valued functions," Teor. Funkcĭ Funkcional. Anal. i Prilożen. **184**(5), 1034–1037 (1969).
[61]Schanz, H. and Smilansky, U., "Spectral statistics for quantum graphs: Periodic orbits and combinatories," Philos. Mag. B **80**(12), 1999–2021 (2000).
[62]Schanz, H. and Smilansky, U., "Combinatorial identities from the spectral theory of quantum graphs," Electron. J. Combin. **8**(2), 16 (2001), a part of Special Issue: In honor of Aviezri Fraenkel on the occasion of his 70th birthday.
[63]Tutte, W. T. and Smith, C. A. B., "On unicursal paths in a network of degree 4," Am. Math. Mon. **48**, 233–237 (1941).
[64]Tanner, G., "Spectral statistics for unitary transfer matrices of binary graphs," J. Phys. Math. Gen. **33**(18), 3567–3585 (2000).
[65]Tanner, G., "Unitary-stochastic matrix ensembles and spectral statistics," J. Phys. Math. Gen. **34**(41), 8485–8500 (2001).
[66]van Aardenne-Ehrenfest, T. and de Bruijn, N. G., "Circuits and trees in oriented linear graphs," Simon Stevin **28**, 203–217 (1951).
[67]Weidenmüller, H. A., *Massive Modes for Quantum Graphs* (Springer International Publishing, Cham, 2020), pp. 341–357.